Nanoscale

PAPER

Cite this: *Nanoscale*, 2017, **9**, 7169

Combining light-harvesting with detachability in high-efficiency thin-film silicon solar cells†

Sanjay K. Ram, *[a] Derese Desta, [b] Rita Rizzoli, [c] Michele Bellettato,[b] Folmer Lyckegaard,[a] Pia B. Jensen,[a] Bjarke R. Jeppesen,[a] Jacques Chevallier,[a] Caterina Summonte,[b] Arne Nylandsted Larsen[a] and Peter Balling [a]

Received 26th January 2017,
Accepted 7th May 2017

DOI: 10.1039/c7nr00658f

rsc.li/nanoscale

Efforts to realize thin-film solar cells on unconventional substrates face several obstacles in achieving good energy-conversion efficiency and integrating light-management into the solar cell design. In this report a technique to circumvent these obstacles is presented: transferability and an efficient light-harvesting scheme are combined for thin-film silicon solar cells by the incorporation of a NaCl layer. Amorphous silicon solar cells in p-i-n configuration are fabricated on reusable glass substrates coated with an interlayer of NaCl. Subsequently, the solar cells are detached from the substrate by dissolution of the sacrificial NaCl layer in water and then transferred onto a plastic sheet, with a resultant post-transfer efficiency of 9%. The light-trapping effect of the surface nanotextures originating from the NaCl layer on the overlying solar cell is studied theoretically and experimentally. The enhanced light absorption in the solar cells on NaCl-coated substrates leads to significant improvement in the photocurrent and energy-conversion efficiency in solar cells with both 350 and 100 nm thick absorber layers, compared to flat-substrate solar cells. Efficient transferable thin-film solar cells hold a vast potential for widespread deployment of off-grid photovoltaics and cost reduction.

Introduction

Thin-film solar cells (TFSC) are being increasingly applied in building-integrated photovoltaics and consumer electronics,[1–3] due to their attractive attributes like potential for roll-to-roll processing,[4] and aesthetic compatibility.[5,6] As the sizes of electronic devices decrease, so does the required electrical power for their operation, making TFSCs ideal for cordless power supplies that harvest ambient light energy in devices like sensors and internet-of-things devices.[7] Amorphous silicon (a-Si : H) TFSCs are particularly appealing for such applications, because of the mature high-yield and low-cost manufacturing technology. Non-toxicity and compatibility with indoor lighting are additional qualities that make a-Si : H solar cells well-suited for wearable electronics.

Three major interconnected constraints stand in the way of achieving ubiquitous applicability of Si-TFSCs: cost-effectiveness, low energy-conversion efficiency and the difficulty in fabricating solar cells on diverse substrates. Advancement in solar cell technology can increase cost-effectiveness through better and low-cost materials, higher efficiencies, and improved durability. Thinner absorber layers are intricately linked to the cost issue as they increase the cell stability and reduce the material cost, but on the downside, lead to decreased absorption of light and poor efficiencies.[8] Strategies for increasing the utilization of incident light to generate more photocarriers are essential in Si-TFSCs to maximize the current density and energy-conversion efficiency, and especially so in the newer ultra-thin (active layers ≤100 nm thick) solar cells.[9–15] A processing related constraint arises from the fact that fabrication of device-quality silicon thin-films typically requires temperatures in the range of 200–300 °C and substrates with optimized surfaces, commonly glass.[16,17] The glass substrate is one of the factors that contribute to high manufacturing costs,[18] and due to its rigidity, restricts many potential applications of solar cells. Although Si-TFSCs have been fabricated on some uncon-

[a]*Department of Physics and Astronomy-iNANO, Aarhus University, Gustav Wieds vej 14, DK-8000 Aarhus C, Denmark. E-mail: sanjayk.ram@gmail.com, sanjayk.ram@inano.au.dk*

[b]*Department of Physics and I3N, University of Aveiro, Campus Universitário de Santiago, 3810-193 Aveiro, Portugal*

[c]*Istituto per la Microelettronica e Microsistemi (IMM)-Consiglio Nazionale delle Ricerche, via Gobetti 101, 40129 Bologna, Italy*

†Electronic supplementary information (ESI) available: (1) Electron generation rate profile calculated across the a-Si : H layers of the solar cells; (2) the results of SE measurements performed on an *i*-a-Si : H layer; (3) determination of optical bandgap from the absorption coefficient (α) calculated from the R&T spectra of the silicon thin films; (4) the plots of fitted real and imaginary part of the dielectric constant spectra, and the spectral dependence of the refractive indices (n) and the extinction coefficients (k) of the silicon thin films (p, i, n, and buffer layers) along with their optoelectronic properties listed in a table; and (5) the spectral dependence of the n and k of the TCO layers. See DOI: 10.1039/c7nr00658f

ventional substrates,[2,18–20] low-cost mass manufacturing of solar cells with high efficiencies on these substrates are yet to be seen.

The concept of transferable solar cells – devices which can be grown on compatible and optimized substrates, detached and then transferred to other destination surfaces – offers an appealing solution[21] for opening the door to economical substrate-recycling[22] and a plethora of novel low-cost applications. A number of approaches are reported for separating semiconductor thin-films from their underlying substrates.[23–26] The reported techniques of separation of TFSCs from substrates either restrict the kind of primary substrates that can be used (*e.g.*, silicon wafer substrate only) or the configuration of the solar cell (*e.g.*, n-i-p configuration for separation along a Ni interlayer).[27] Applying wet chemical etching process to TFSCs to etch away a temporary growth substrate to create a detachable solar cell has been reported.[28]

As can be expected with a thin-film electronic device, detachment and transfer of solar cells may be detrimental to device integrity and functioning, often leading to low energy-conversion efficiencies.[29,30] Further, detachable TFSCs require a smooth plane of separation over a large area, precluding incorporation of light-trapping nanostructures or nanotextures at the back, which is a crucial part of competitive TFSC technology. In this work, we report high-efficiency detachable solar cells with an integrated light-trapping strategy using a NaCl sacrificial layer between an a-Si : H solar cell and its glass substrate. With experimental and theoretical studies we show that the nanostructured surface grains of as-deposited NaCl leads to light trapping in the solar cell with a consequent significant enhancement of the efficiency. Finally, we demonstrate the detachment of the solar cell from the primary substrate by dissolution of the NaCl layer in water and its transfer to a secondary plastic substrate with retention of high efficiency.

Results

Fabrication, detachment and transfer process

The schematic illustration of the steps involved in the proposed method of fabrication, detachment and transfer of a Si-TFSC is shown in Fig. 1. First, a thin layer of NaCl (500 nm) was deposited at room temperature on a 3.5 × 3.5 cm^2 glass substrate, shown in Fig. 1a. Immediately afterwards, a 100 nm thick encapsulating protective dielectric layer of SiO_2 was deposited on the NaCl layer, shown in Fig. 1b. The front electrodes were fabricated using transparent conducting oxides (TCO), by the sequential deposition of a 220 nm thick indium tungsten oxide (IWO) layer,[31] followed by an 8 nm thick aluminum doped ZnO (AZO) layer to protect the IWO layer from the reducing atmosphere of the H_2 plasma during the solar cell fabrication, shown in Fig. 1c.

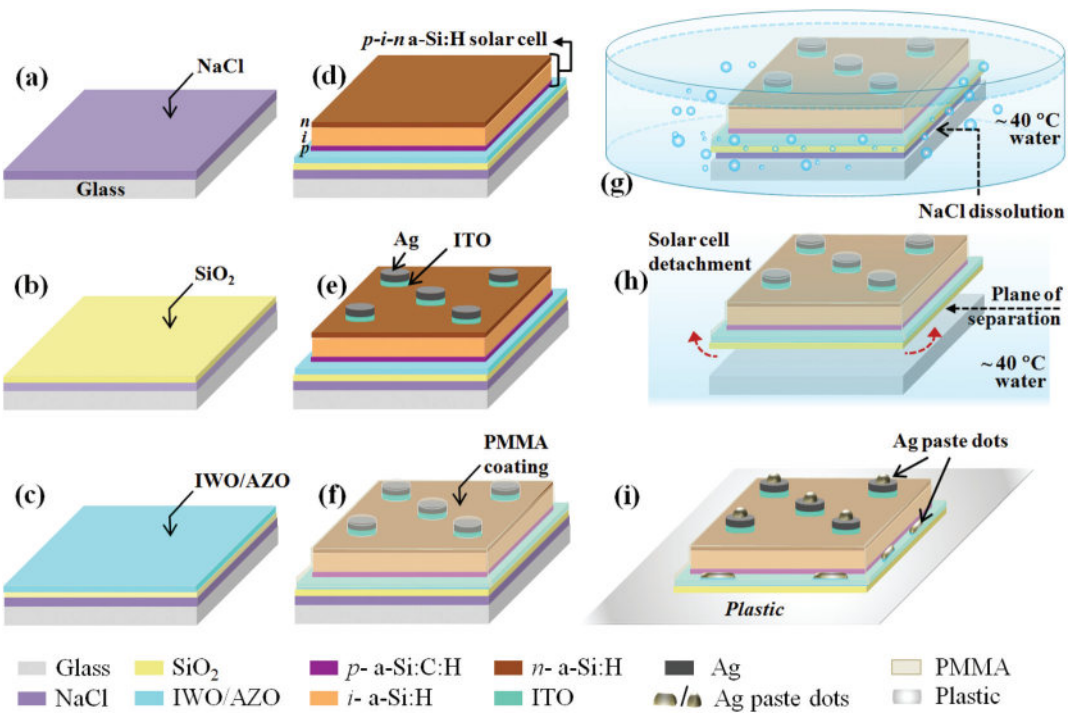

Fig. 1 Schematic illustration of the steps involved in the proposed technique for transferring solar cells from the growth substrate (glass) to an unconventional substrate (plastic sheet in this report): (a) deposition of sacrificial NaCl layer on a glass substrate, (b) deposition of SiO_2 barrier layer, (c) front-electrode TCO (IWO/AZO) coatings, (d) p-i-n type a-Si : H solar cell deposition, (e) back-electrode ITO/Ag deposition, (f) spin-coating of a thin PMMA layer to protect the solar cell structure, (g) immersion of the device assembly in warm water (~40 °C) to enable quick dissolution of the NaCl layer, (h) detachment of the solar cell from the glass substrate, (i) attachment of the free-standing solar cell to a plastic sheet.

The a-Si : H solar cells were grown in a superstrate configuration (p-i-n type) in a cluster-type radio frequency plasma-enhanced chemical vapor deposition (RF-PECVD) reactor, at 13.56 MHz. Fig. 1d shows the a-Si : H solar cells on the NaCl/SiO_2/TCO-coated substrates. The deposition conditions were optimized for obtaining conformal growth of the silicon layers over the nanotextured surface. For comparison, reference solar cells (not shown in Fig. 1) were also fabricated under the same deposition conditions on a similar TCO-coated flat glass substrate and on a commercially available textured Asahi substrate (glass substrate coated with SnO_2 : F).[32] In this work, two sets of solar cells were fabricated and studied, one with cells having conventional thickness (300–350 nm) of absorber layers, and the other set with cells having ultra-thin (100 nm) absorber layers. Hereafter, the conventional thickness solar cells are denoted as SC, while the ultra-thin solar cells are denoted as USC, for all the three kinds of substrates, namely, NaCl-coated glass (NaCl-SC and NaCl-USC), untextured glass (Flat-SC and Flat-USC) and Asahi (Asahi-SC and Asahi-USC). Finally, for the back electrical contacts to the devices, a 30 nm thick indium-tin-oxide (ITO) layer followed by a 200 nm Ag layer were deposited through a metallic shadow mask with 3 mm diameter holes to obtain multiple circular solar cells on the same glass substrate, as depicted in Fig. 1(e).

Fig. 1(f–i) illustrate the steps of detachment and transfer of the solar cell. An inevitable concern in a layer-dissolution approach is to prevent the device from being exposed to any solvents (water in our case) during the dissolution of the sacrificial layer. To this end, a final protective layer of polymethyl methacrylate (PMMA) was spin-coated on the solar cells, schematically shown in Fig. 1f. Since the PMMA layer covers the cell up to the edges of the substrate, a linear scratch was applied on the solar cell, ~1 mm inside of the edges along the four sides of the substrate to create a channel through which water could come in contact with the NaCl layer. The sample was immersed in water preheated to ~40 °C to facilitate dissolution of the NaCl layer, which led the solar cell to be detached from the underlying substrate within a few seconds and float up, as shown schematically in Fig. 1g and h. The free-floating solar cell was removed with wooden spatulas and placed on an inexpensive plastic sheet coated with PMMA. After the transfer, a polydimethylsiloxane (PDMS) block with an anti-sticking coating was placed on the solar cell for application of slight and evenly distributed pressure. The sheet was baked in a convection oven at 50 °C for 30 minutes. Finally, acetone soaked clean-room swabs were used to remove selectively the PMMA layer over the back-contacts and over the extending TCO strip to expose the metal area and TCO underneath, respectively. Dots of silver paste were applied on top of the exposed TCO area and the back-contacts to enable good electrical contacts. Fig. 1i shows the transferred solar cell with its contacts.

Structural analyses of surfaces and interfaces

Fig. 2a shows the surface topography of the NaCl/SiO_2-coated substrate studied by atomic force microscopy (AFM). This surface reveals a nanotextured appearance, with paraboloid-shaped surface grains, ~300 nm in diameter at the base. The height of these surface grains is ~100 nm and the root mean square surface roughness (σ_{rms}) is ~18 nm. The surface topography of the substrate after coating consecutively with IWO and AZO on top of NaCl is shown in Fig. 2b. The surface roughness is seen to be maintained and the morphology of the nanotextured surface also retained after the coating of the TCO layers, due to the fact that the IWO layer is amorphous in nature and grows conformally.[31] In Fig. 2c the surface morphology of the Asahi substrate is shown for comparison. The textured Asahi surface with σ_{rms} ~ 43 nm is composed of a few large pyramidal-shaped surface grains with base width approximately 700–900 nm and clusters of small-sized grains approximately 50–70 nm. Visually, the surfaces of the NaCl coated substrate and the Asahi substrate are quite similar to

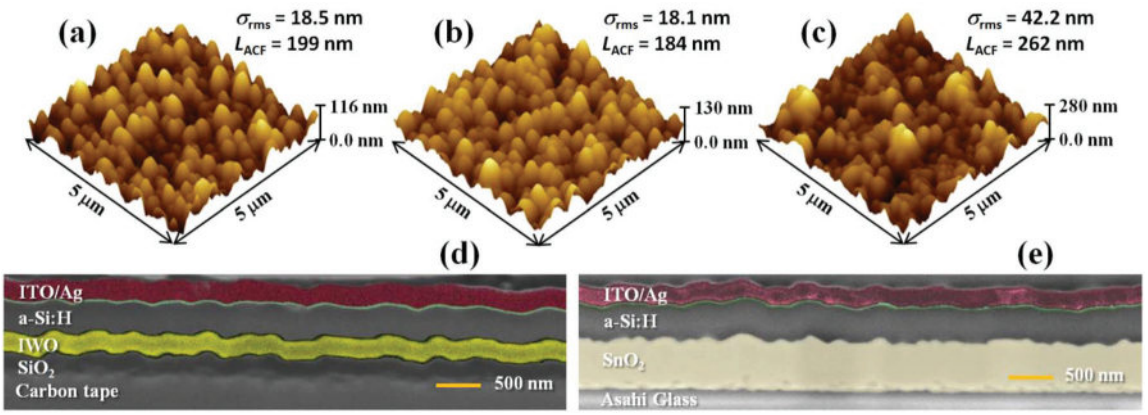

Fig. 2 AFM images of the surface morphologies (5 μm × 5 μm) of (a) the glass/NaCl/SiO_2 surface, (b) the surface of the same substrate after rf-MS deposited 220 nm IWO and 10 nm AZO layers, and (c) a commercial Asahi (SnO_2 : F) substrate. The images shown in (d) and (e) correspond to the cross-sections of FIB milled transferred NaCl-SC and Asahi-SC, respectively. Different layers are shown in false color for better visualization and identification of the device structure.

each other with the exception of the large grains on the Asahi surface. To further ascertain the random distribution of the nanostructured features on the surface, we turn to the autocorrelation function, which expresses how the surface is correlated to itself at a certain distance.[33] The deduced autocorrelation lengths (L_{ACF}) for the TCO coated NaCl and Asahi are 184 nm and 262 nm, respectively.

Scanning-electron-microscopy (SEM) images of the focused-ion-beam (FIB) milled cross-section of NaCl-SC and Asahi-SC are shown in Fig. 2d and e, respectively. It is evident from the cross-sectional analyses that the nanostructured features of the NaCl surface are retained in each layer, throughout the solar cell growth, similar to what is observed in the surface analyses. The interface of SiO_2/NaCl seems to be slightly distorted after dissolving the NaCl; however, no such deformity or distortion can be noticed at the SiO_2/TCO interface.

Optical performance of solar cells

The total optical absorption of the complete p-i-n a-Si : H solar cells (conventional and ultra-thin) with a back-reflector is calculated from the measured total reflection as (1 − total reflection)%. In Fig. 3a the absorption spectra of the NaCl-SC, the Flat-SC and the Asahi-SC having ~300 nm thick i-layers are presented. The optical absorption of the Asahi-SC is, as expected, higher than that of the Flat-SC, owing to the optimized surface textures in the Asahi substrate. Textured SnO_2 Asahi substrates are popular as light trapping substrates in solar cell manufacturing. In this work, Asahi ANS10ME substrates are used, which have a better light-scattering and electrical mobility than Asahi U.[32] A similar broadband enhancement in the optical absorption can be observed in the NaCl-SC with the major enhancement in the absorption occurring in the long wavelength region (>600 nm). In Fig. 3b the wavelength dependence of the total optical absorption of the ultra-thin solar cells: the NaCl-USC, the Asahi-USC and the Flat-USC (~100 nm thick i-layer) are shown. The onset of a noticeable improvement in the absorption spectra of the NaCl-USC device with respect to the Flat-USC is seen to be around λ = 500 nm, because light at and beyond this wavelength penetrates the solar cell to reach the back-reflector surface in these ultra-thin solar cells and the advantage of the textured surfaces over the planar surfaces becomes evident.[34] The increased optical absorption in the long-wavelength region is apparent in both NaCl-SC and NaCl-USC, demonstrating the light-trapping benefit of the nanostructured surface over the flat substrate.

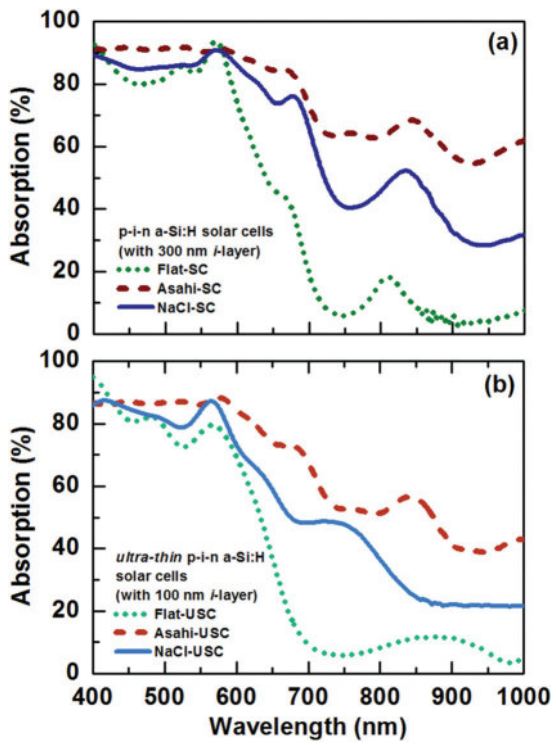

Fig. 3 Optical absorption spectra of (a) the solar cells with 300 nm i-layers, deposited on Flat, Asahi (ANS10ME) and NaCl-coated substrates, (b) the ultra-thin solar cells with 100 nm i-layer deposited on Flat and NaCl-coated substrates.

FDTD numerical simulation

An optical modeling study using finite-difference time-domain (FDTD) simulation software from Lumerical[35] was carried out to calculate the absorption profiles of the solar cells on the flat and the nanostructured NaCl surfaces (Flat-SC and NaCl-SC) for wavelengths 400–800 nm. The details of the simulation model can be found in the Experimental section. Fig. 4a compares the simulated optical absorption spectra of the p-i-n a-Si : H Flat-SC and NaCl-SC for a 300 nm thick i-layer. The simulations agree qualitatively with the experimental data (Fig. 3a) and the basic spectral shape is well reproduced by the optical model. In particular, the enhancement of the optical absorption at the long wavelengths for the NaCl-SC compared to the Flat-SC is qualitatively similar. The optical absorption spectra of the Flat-SC are reproduced excellently in the simulation, while the simulated absorption in the NaCl-SC is somewhat lower than the experimental measurements. This difference arises from non-idealities in the simulation parameters, and the non-uniform optical variations (compared to simulations) in the nanostructured surfaces/interfaces along the *z*-direction. The nanograins are implicitly assumed to be perfectly homogeneous along the *z*-direction in the simulations carried out in 2D (*xy*-plane). Also, the refractive indices and thicknesses of the materials grown over the textured surfaces can deviate slightly from the assumed values obtained from materials grown on flat growth surfaces.

The distribution of the simulated optical absorption densities in the layers of the solar cells NaCl-SC and Flat-SC are shown for 650 nm and 735 nm light in Fig. 4b and c, respectively. The Flat-SC device shows regions of high and low optical absorptions at these long wavelengths arising from Fabry–Perot resonances within the film. In case of interfaces and reflectors that acquire nanotextures from the nanostructured NaCl surface underneath, such a strong interference effect is not seen because the structured back reflector induces a field with a range of propagation directions and non-trivial phase

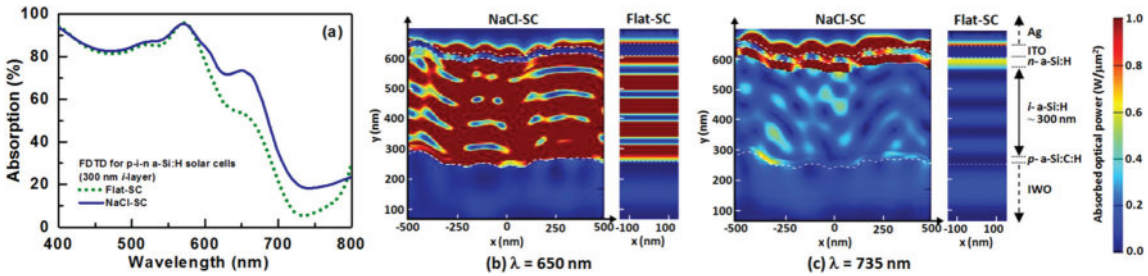

Fig. 4 (a) Optical absorption as a function of wavelength, calculated by FDTD modelling for the Flat-SC and the NaCl-SC having 300 nm thick i-layers. The calculated optical absorption distribution profiles of the p-i-n a-Si : H thin-film solar cells (Flat-SC and NaCl-SC) are shown for two long wavelengths: (b) λ = 650 nm and (c) λ = 735 nm. In these images the light propagates in the +ve y direction and the polarization of the light is in the x-direction. The dotted lines are added to demarcate the a-Si : H thin-film from the top and bottom TCOs.

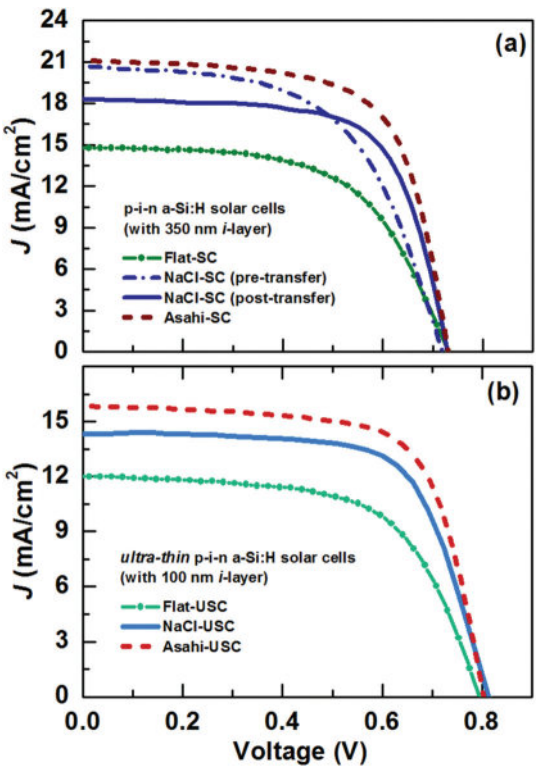

Fig. 5 (a) The J–V characteristics, under AM 1.5 direct solar spectrum, 100 mW cm^{-2} irradiation, of the p-i-n a-Si : H Flat-C, Asahi-SC, NaCl-SC (pre-transfer) and NaCl (post-transfer). (b) The J–V characteristics of ultra-thin solar cells: Flat-USC, Asahi-USC and NaCl-USC.

delays. This leads to the visible spatial inhomogeneity of the absorption in the NaCl-SC. At λ = 735 nm, the absorption profile of the Flat-SC shows an overall low absorption, whereas in the NaCl-SC, localized higher absorption regions are visible throughout the a-Si : H absorber layer. The parasitic absorption near the back-reflector is enhanced in the long wavelength region, due to the nanotextured Ag layer. These parasitic losses associated with textured Ag surfaces are well-studied in literature.[34,36–38] The solar-spectrum-weighted electron generation rate profiles calculated across the a-Si : H layers of the Flat-SC, and NaCl-SC devices are shown in Fig. S1 of the ESI.†

Photovoltaic performance of TFSCs

In Fig. 5a we present the J–V characteristics of the solar cells (Flat-SC, NaCl-SC and Asahi-SC) with 350 nm i-layers deposited in the same run of the PECVD system, measured under AM 1.5 direct spectrum, 100 mW cm^{-2} solar irradiation. The solar-cell device parameters such as short-circuit current density (J_{sc}), open-circuit voltage (V_{oc}), fill-factor (FF) and energy-conversion efficiency (η) are listed in Table 1. The reference cell, Flat-SC, yielded an energy-conversion efficiency of 6.4% with a J_{sc} of 14.8 mA cm^{-2}. The J–V characteristic of one of the pre-transfer NaCl-SC (with the NaCl interlayer still intact between the solar cell and the original growth substrate) having the best efficiency of 8.5% with a J_{sc} of 20.7 mA cm^{-2}, is shown in Fig. 5a with a dashed-dotted line. The pre-transfer and post-transfer solar cell parameters were measured on circular devices, at different locations on the same substrate. The J–V

Table 1 The device parameters obtained from J–V characteristics of the p-i-n a-Si : H solar cells with 350 nm and 100 nm thick i-layers. The enhancements in J_{sc} and η are calculated using $\Delta J_{sc} = [(J_{sc\text{-textured-SC}} - J_{sc\text{-Flat-SC}})/J_{sc\text{-Flat-SC}}] \times 100\%$ and $\Delta\eta = [(\eta_{textured\text{-SC}} - \eta_{Flat\text{-SC}})/\eta_{Flat\text{-SC}}] \times 100\%$, respectively

a-Si : H p-i-n devices	Substrate	i-layer (nm)	V_{oc} (mV)	FF (%)	η (%)	$\Delta\eta$ (%)	J_{sc} (mA cm^{-2})	ΔJ_{sc} (%)
Flat-SC (reference)	Glass/TCO	350	731	59	6.4	—	14.8	—
Asahi-SC	Asahi-SnO_2 : F	350	730	67	10.3	61.0	21.1	42.6
NaCl-SC (pre-transfer)	Glass/NaCl/SiO_2/TCO	350	719	57	8.5	32.8	20.7	40.0
NaCl-SC (post-transfer)	Plastic sheet	350	729	68	9.0	40.6	18.3	24.0
Flat-USC (reference)	Glass/TCO	100	795	62	5.9	—	12.0	—
Asahi-USC	Asahi-SnO_2 : F	100	803	69	8.8	49.2	15.8	31.9
NaCl-USC	Glass/NaCl/SiO_2/TCO	100	813	69	8.0	35.6	14.3	19.2

characteristic of a transferred NaCl-SC, characterized after attachment to the plastic sheet, is shown with a solid line in Fig. 5a. A maximum efficiency of 9% and J_{sc} of 18.3 mA cm^{-2} were obtained from the transferred solar cell. The Asahi-SC showed an efficiency of 10.3% with a J_{sc} of 21.1 mA cm^{-2}, indicating the superior quality of the solar cell and effectiveness of the deposition conditions in ensuring conformal growth.

The *J–V* characteristics of the ultra-thin solar cells (Flat-USC, NaCl-USC and Asahi-USC) are presented in Fig. 5b and the device parameters are given in Table 1. The Flat-USC device revealed an efficiency of 5.9% and a J_{sc} of 12.0 mA cm^{-2}. The efficiency of the Flat-USC is very close to its thicker counterpart and the loss of J_{sc} due to the reduced thickness is compensated with the improved V_{oc}. The NaCl-USC achieved an efficiency of 8% and a J_{sc} of 14.3 mA cm^{-2}. The Asahi-USC shows η = 8.8% and J_{sc} = 15.8 mA cm^{-2}.

Discussion

In our study, a very thin NaCl layer (50–200 nm) led to difficulties during the transfer process, resulting in cracks and patchy detachment of cells (results not shown here). Instead, for the glass substrate used in the present investigation, the optimum thickness of NaCl layer was found to be ~500 nm which allowed an easy detachment of the solar cell. The potential of water dissolvable NaCl epitaxial interlayers (grown at high temperatures on preferred crystalline orientated substrates) for detaching epitaxially grown small area thin-films structures was recognized decades ago,[25] as was the usefulness of NaCl single crystal substrates for growing epitaxial thin-films.[26,39,40] However, in our work, the epitaxial characteristic of NaCl is not required, and a low-cost thermally-evaporated layer of NaCl is sufficient to create the sacrificial layer over a large area. Organic materials like polyvinyl acetate (PVA),[41] and NaCl,[25,26] both water soluble, have been reported for the separation of semiconductor materials from their growth substrates but unlike NaCl (with a high melting point of 801 °C),[39] PVA is not capable of withstanding the Si-TFSCs fabrication process. A sacrificial layer made of the NaCl thin-film is chemically inert, electrically non-conducting, and can be simply dissolved in water in a quick and non-toxic process. Wet chemical etching of metal layers is expensive and time-consuming, and potentially damaging to the undersurface of the solar cell. In contrast, the NaCl-based detachment offers another industrially relevant advantage in that the substrate is minimally damaged and can be prepared for a next cycle of solar cell deposition with a very low cost-per-substrate-reuse cycle.[22]

As seen in Fig. 1, a SiO_2 layer separates the NaCl layer from the rest of the solar cell. The SiO_2 layer in this approach acts as both a barrier layer as well as a supporting layer, and is a crucial and distinguishing feature. During the silicon deposition, the SiO_2 layer prevents contamination with Na, which can be detrimental to the TFSC.[42] It also protects the NaCl layer from the humidity in the atmosphere and the subsequent layers of semiconductor materials from any structural or functional damage from the underlying NaCl and any impurities therein.[43] The electrical transport properties of the TCO coated on the substrates remained unchanged even after the substrates were stored in ambient conditions in the laboratory for several weeks, indicating that the SiO_2 barrier layer between the NaCl and the TCOs helps to maintain the stability of the substrate (see the Experimental section).

The SiO_2 layer also provides a stable undersurface for the TCO and the overlying solar cell structure after the NaCl is dissolved away. A disturbance or disruption of material is inevitable at the plane of separation between thin-films. However, this disruption can be minimized or the plane of separation can be shifted away from the thin-films stack that is going to be transferred by using protective interlayers. In this approach, the SiO_2 layer functions both to protect the overlying layers and to shift the plane of separation away from the solar cell. Thus, we can see in Fig. 2d that the interface of SiO_2/NaCl seems to be slightly distorted after dissolving the NaCl; however, no such deformity or distortion can be noticed at the SiO_2/TCO interface. The SiO_2 layer has no role in the electrical performance of the solar cell, and therefore is a sacrificial layer that bears the impact of the separation process, leaving behind the solar cell unaffected. In terms of industrial adaptability, the SiO_2 layer is compatible with in-line solar cell manufacturing processes.

The light-trapping effect in the solar cells brought about by the surface nanotextures of the NaCl layer is a determinative factor that boosts the commercial viability of the present approach significantly. The surface morphology of the 500 nm thick NaCl layer studied with AFM (Fig. 2a and b) shows paraboloid shaped surface grains (~300 nm base diameter and ~100 nm in height) randomly distributed over the surface. The near-conformal deposition of the solar cell layers results in nanotexturing up to the back of the NaCl-SC leading to a nanotextured back-reflector. The observed broadband absorption enhancement in both the conventional thickness and ultra-thin p-i-n solar cells fabricated on the NaCl coated substrates thus arises from a combination of in-coupling of short-wavelength light at the front and effective scattering of longer wavelength light at the internal interfaces and the back.[44] The light-trapping effect observed experimentally is also corroborated by our simulation studies, Fig. 4. To our knowledge, neither the morphology of thermally-deposited multilayer NaCl film as thick as few hundreds of nanometers nor the effect of the roughness of the NaCl layer on the optoelectronic properties of overlying semiconductor layers is explored in the literature, but few studies reveal the optical behavior of similar features. Periodic paraboloid nanoscale protuberances (200 nm base diameter and 70 nm height) were previously explored for anti-reflection properties in n-i-p a-Si : H TFSCs and shown to improve the in-coupling of the incident light into solar cells.[45] A back-reflector on nanocone-shaped a-Si : H features (150 nm height of cones) with a flat front surface was reported to provide light-trapping effects at longer wavelengths.[46]

The similarity between the photocurrent densities of the solar cells fabricated on the NaCl-coated substrates and on the

Asahi substrates in Fig. 5 implies that the nanotextured surface of the NaCl has an efficient photon-harvesting effect without any noticeable deterioration of the electrical properties of the solar cells (Table 1). According to theoretical studies by Tamang *et al.*,[44] a 24% enhancement in the J_{sc} in a multiscale textured single junction p-i-n (μc-Si : H) solar cell with a 500 nm period/base-width of the textured back-reflector is possible if the periods/base-width of the front textures are in the range of 100–500 nm. This is similar to the 300 nm–500 nm sized features inherently present in the NaCl-coated substrate solar cells in this work, and can be expected to be at least equally effective for light-trapping in a-Si : H solar cells.

It is known that apart from the height of the nanoscale features in the random textured system (quantified by roughness, σ_{rms}), the spatial distance between the adjacent features (understood from the autocorrelation length, L_{ACF}) also determine the optical effects of as well as material growth over the features.[47–49] The simultaneous dependence of photocurrent generation on both the L_{ACF} and the σ_{rms} was reported for c-Si and μc-Si : H solar cells, revealing that optimal combinations of these two parameters are effectively responsible for the current.[49] In this study, it was shown that at a fixed σ_{rms} the J_{sc} shows a bell-shaped dependence on the L_{ACF}, so that for a certain height of roughness there can be a range of values of L_{ACF} that lead to equivalent J_{sc}. In our study, the σ_{rms} = 43 nm and L_{ACF} = 262 nm in Asahi and the σ_{rms} = 18 nm and L_{ACF} = 184 nm in NaCl coated substrate denote smaller and more close-set features in the latter, but an optimal balance between the two parameters lead to a good J_{sc} in the NaCl-SC in spite of smaller features.

The NaCl-SC shows significant improvements of 32.8% and 40% in the efficiency and the short-circuit current density, respectively, compared to the reference Flat-SC. The post-transfer efficiency of 9% is the highest among all reported transferred thin-film solar cells, and close to the best reported efficiency in the category of single-junction a-Si : H TFSCs without any additional conventional light-management techniques, to our knowledge.[15,50–52] Particularly remarkable is the improvement of the performance in the 100 nm i-layer ultra-thin solar cells on NaCl substrate, where enhancements of 35.6% in the efficiency and 19.2% in the J_{sc} are seen in the NaCl-USC compared to the Flat-USC. The performance of the ultra-thin solar cell is also, to our knowledge, a first time reported 8% efficiency for a transferrable, ultra-thin (100 nm i-layer), single junction a-Si : H solar cell.

As seen from Table 1, the V_{oc} in the transferred and the reference Flat and Asahi cells are ~730 mV, which we believe can be further improved by optimization of the solar cell layers. There can be a number of reasons responsible for a low V_{oc}, like the low bandgap of the intrinsic layer, presence of defects in the absorber layer, the Fermi level position of the doped layers, work function of the TCOs, and untreated and defective p/i and n/i interfaces.[53–56] While a high hydrogen dilution in silane leads to a better material quality and improvement in the optical bandgap of the absorber layer, it also leads to poor conformality of the layers over textured surfaces. A higher H_2 dilution can also lead to formation of microcrystalline phase on textured surfaces, lowering the bandgap and therefore the V_{oc}. We have tried to maintain a balance between the material quality and conformal growth by using a lower deposition temperature along with low H_2 dilution (Fig. S2–S4†). In our intrinsic amorphous silicon material, the bandgap is around 1.7 eV as confirmed by both spectroscopic ellipsometry (SE) and reflection and transmission (R&T) studies. Comparing the ultra-thin solar cells with the cells having conventional thickness i-layers, the role of the thick i-layer (350 nm) in decreasing the V_{oc} becomes evident. The V_{oc} of the ultra-thin a-Si : H solar cells on planar substrate with 100 nm thick i-layer is ~795 mV, which is 64 mV higher than that of the thick Flat-SC. Similarly, there are improvements in the V_{oc} by 70–80 mV in NaCl-USC and Asahi-USC. There are two possible factors that contribute to lower V_{oc} in the cell with the thicker i-layer: the increase in the number of defects and the reduction in the built-in potential in the thicker absorber layers.[53]

The unexpectedly lower FF of the solar cells (both conventional and ultra-thin) on the flat substrates compared to the nanostructured NaCl coated substrate possibly originates from the difference between the thicknesses of the electrically resistive protective AZO layers in the solar cells on flat and NaCl substrates. The short growth time fixed by estimating the deposition of ~8 nm layer thickness over a flat surface may lead to lower thickness of the layer over a textured surface. Likewise, the buffer layer determined to be optimal for the textured surfaces may result in a thicker layer for the planar devices keeping the same deposition duration. Overall, a thinner i-layer and judicious use of buffer and barrier layers can further improve the solar cell performance and the transfer process.[55,56]

The core concept of dissolution of a NaCl interlayer is universal enough to be applicable to a broader range of devices without any major changes in the existing manufacturing process or the solar cell architecture, or a need for additional sophisticated machining. The approach presented here can be adapted to n-i-p solar cells by replacing the TCO layer with a metal (Ag or Al) layer, as well as to Si-TFSCs on other growth substrates like metal foils.

Conclusion

We demonstrated a simple, low-cost and scalable approach to detach silicon thin-film solar cells from their growth substrates by water-based dissolution of a sacrificial NaCl layer, while simultaneously harnessing the light-trapping effect in the solar cell grown on the nanotextured surface of the NaCl layer underneath. The effective light-harvesting brings about remarkable enhancements in the short-circuit current density of p-i-n a-Si : H solar cells on the NaCl coated substrate – 40% in conventional thickness solar cells and 19.2% in ultra-thin solar cells, and significant enhancement in the efficiencies of both, compared to their planar substrate counterparts.

Preservation of the energy-conversion efficiency after the transfer process, and compatibility with the existing solar cell manufacturing processes including roll-to-roll processing are salient advantages of our NaCl based detachment technique. We achieved 9% post-transfer efficiency in the solar cell on a low-cost plastic sheet, which is the highest efficiency reported to our knowledge in an a-Si : H solar cell detached and transferred by any method. Highly efficient transferable thin-film solar cells with a built-in light-trapping scheme offer a practical route to achieving solar cell integration with surfaces of sundry materials. The transfer of optimally fabricated photovoltaic devices to unconventional surfaces can enable ultra-lightweight affixable solar cells which are anticipated to open up diverse integration and application possibilities.

Experimental section

Interlayer fabrication

The sacrificial NaCl layer was deposited on a pre-cleaned and baked glass BOROFLOAT® 33 glass substrate (3.5 × 3.5 cm^2) at room temperature by a thermal evaporation technique. NaCl was heated by means of a resistance foil made from refractory material (W or Mo). The distance between the source and the substrate was 13 cm. A protective SiO_2 layer was subsequently deposited by an electron-beam-evaporation technique. The distance between the source and the substrate was 20 cm.

Front-electrode coatings[31]

The TCOs (IWO and AZO) were deposited by an rf-magnetron sputtering (rf-MS) technique at room temperature. The IWO layer deposition was performed using an In_2O_3 ceramic target containing 1 wt% WO_3, at 40 W rf power and 2.25 mTorr pressure of an Ar + O_2 gas mixture, where the O_2 dilution in Ar is 0.75%. The AZO layer was deposited using a ZnO ceramic target containing 2 wt% Al_2O_3, at 100 W rf power and 2.25 mTorr Ar pressure. The resistivity of the TCO double layer (IWO + AZO) deposited on the glass substrate was ~5.5×10^{-4} Ω cm. The TCO layers overlying the NaCl and SiO_2 layers were characterized by low resistivity ~4×10^{-4} Ω cm and high optical transparency above 85% in the visible light range, implying no significant adverse influence of the surface morphology of the TCO layers.

Solar cell fabrication[13,48]

The p-i-n type a-Si : H TFSCs were grown in an RF-PECVD cluster-type system in the temperature range of 120 °C to 170 °C (measured on the substrate). The p-i-n solar cells were deposited using specific gas mixtures for each layer, in order to obtain the desired optical and electrical properties, in the following sequence: (1) an 18 nm p-type a-Si : C : H window layer, using a (SiH_4 + H_2 + B_2H_6 + CH_4) gas mixture, (2) a 3–6 nm thick undoped a-Si : C : H buffer layer, using (SiH_4 + CH_4 + H_2), (3) a 100–350 nm thick intrinsic (*i*) a-Si : H layer, using (SiH_4 + H_2) and (4) a 35 nm thick n-type a-Si : H layer, using a (SiH_4 + H_2 + PH_3) mixture.

Back-electrode coatings

A 30 nm thick ITO layer was first sputtered using an In_2O_3 ceramic target containing 10 wt% SnO_2 at 150 °C, 40 W rf power and 14 mTorr Ar pressure, followed by a thermally evaporated 200 nm thick Ag layer to provide the back electrical contacts to the devices.

Characterization studies[13,48]

The surface topography of the substrates was studied using atomic force microscopy (AFM, Bruker Dimension Edge) and the cross-sectional analysis of the solar cell devices was carried out using a focused ion beam instrument (FIB, FEI VERSA 3D). Spectroscopic ellipsometry (Sentech 850 PV) technique was employed to study the structural compositions of the silicon (p, i, n and buffer layers) and the TCO (ITO and IWO) thin films and obtain their optical parameters. The R&T measurements were carried out on the silicon thin films, the TCOs and the solar-cell devices using a spectrometer equipped with a 150 mm integrating sphere (PerkinElmer Lambda 1050). The optical, structural and optoelectronic properties of the silicon thin film layers of the solar cells can be found in Fig. S2–S4 and in the Table S1 in the ESI.† The solar cell current density *vs.* voltage (*J*–*V*) characteristics under one sun illumination were measured at 100 mW cm^{-2} AM1.5 irradiance using a calibrated Oriel solar simulator with a xenon arc lamp. The light is irradiated over the whole area of the sample through the glass/plastic side. The device diameter is 3 mm as determined by the back-contact-reflector dimension and the spacing between the devices (from edges) is 1.5 mm. For the NaCl-SC, the (*J*–*V*) characteristics of a few randomly chosen cells were carried out before the transfer to minimize pre-transfer handling and accidental scratch damage.

FDTD optical modeling

The AFM topographical data of the NaCl-coated substrate were imported into the simulation to model the realistic solar cell architecture. For simplicity, a conformal coating with the consecutive TCOs, and the doped and the intrinsic a-Si : H layers was considered. The thicknesses of the layers were estimated from the growth rates of the individual layers and with the help of the cross-sectional FIB-SEM images of the fabricated devices. A periodic boundary condition with a period of 1 μm was used in the *x*-direction and perfectly matched layer boundary conditions were applied in the *y*-direction. A broadband EM plane wave (400–800 nm) propagates into the simulation region in the positive *y*-direction. The final absorption data is averaged for the values obtained for parallel and orthogonal polarization. The refractive indices of all layers except the Ag were obtained from SE and R&T measurements (Fig. S4 and S5†). The optical data for Ag was taken from literature.[57] Details of the simulation methodology can be found in our previously reported works.[13,48]

Conflict of interest

The authors declare no competing financial interests.

Acknowledgements

Author Sanjay K. Ram would like to dedicate this work to his father Mr Kashi Nath Ram in his memory. This project is supported by the Danish Strategic Research Council under the project "Thin-film solar cell based on nanocrystalline silicon and structured backside reflectors (THINC)" and by the Innovation Fund Denmark under the project 'SunTune'. We thank Harish Lakhotiya for the optical measurements of the solar cells and Bruno P. Falcão for his support during solar cell characterization studies.

References

1 M. Pagliaro, R. Ciriminna and G. Palmisano, *ChemSusChem*, 2008, **1**, 880.
2 M. B. Schubert and J. H. Werner, *Mater. Today*, 2006, **9**, 42.
3 K. Takei, S. Harada, W. Honda, Y. Yamamoto, K. Kanao, T. Arie and S. Akita, in *Proc. 4th International Conference, DUXU 2015, Part II, USA*, ed. A. Marcus, 2015, p. 675, DOI: 10.1007/978-3-319-20898-5_64.
4 S. Guha, J. Yang and B. Yan, *Sol. Energy Mater. Sol. Cells*, 2013, **119**, 1.
5 J. Carabe and J. J. Gandia, *Opto-Electron. Rev.*, 2004, **12**, 1.
6 S. Y. Myong and S. W. Jeon, *Sol. Energy Mater. Sol. Cells*, 2015, **143**, 442.
7 Y. Ichikawa, T. Yoshida, T. Hama, H. Sakai and K. Harashima, *Sol. Energy Mater. Sol. Cells*, 2001, **66**, 107.
8 T. Matsui, K. Maejima, A. Bidiville, H. Sai, T. Koida, T. Suezaki, M. Matsumoto, K. Saito, I. Yoshida and M. Kondo, *Jpn. J. Appl. Phys.*, 2015, **54**, 08KB10.
9 *Photon Management in Solar Cells*, ed. R. B. Wehrspohn, U. Rau and A. Gombert, Wiley-VCH Verlab GmbH & Co. KGaA, 1st edn, 2015.
10 H.-P. Wang, D.-H. Lien, M.-L. Tsai, C.-A. Lin, H.-C. Chang, K.-Y. Lai and H. He Jr., *J. Mater. Chem. C*, 2014, **2**, 3144.
11 M. L. Brongersma, Y. Cui and S. Fan, *Nat. Mater.*, 2014, **13**, 451.
12 C. F. Guo, T. Sun, F. Cao, Q. Liu and Z. Ren, *Light: Sci. Appl.*, 2014, **3**, e161.
13 S. K. Ram, R. Rizzoli, D. Desta, B. R. Jeppesen, M. Bellettato, I. Samatov, Y. C. Tsao, S. R. Johannsen, P. T. Neuvonen, T. G. Pedersen, R. N. Pereira, K. Pedersen, P. Balling and A. N. Larsen, *J. Phys. D: Appl. Phys.*, 2015, **48**, 365101.
14 V. E. Ferry, M. A. Verschuuren, H. B. T. Li, E. Verhagen, R. J. Walters, R. E. I. Schropp, H. A. Atwater and A. Polman, *Opt. Express*, 2010, **18**, A237.
15 F. J. Haug and C. Ballif, *Energy Environ. Sci.*, 2015, **8**, 824.
16 A. Matsuda, *Jpn. J. Appl. Phys.*, 2004, **43**, 7909.
17 J. Schmidtke, *Opt. Express*, 2010, **18**, A477.
18 H. Águas, S. K. Ram, A. Araújo, D. Gaspar, A. Vicente, S. A. Filonovich, E. Fortunato, R. Martins and I. Ferreira, *Energy Environ. Sci.*, 2011, **4**, 4620.
19 J. K. Rath, in *Advanced Silicon Materials for Photovoltaic Applications*, ed. S. Pizzini, John Wiley and Sons Ltd, 2012, ch. 9.
20 J. Plentz, G. Andrä, T. Pliewischkies, U. Brückner, B. Eisenhawer and F. Falk, *Mater. Sci. Eng., B*, 2016, **204**, 34.
21 C. H. Lee, D. R. Kim and X. Zheng, *ACS Nano*, 2014, **8**, 8746.
22 J. S. Ward, T. Remo, K. Horowitz, M. Woodhouse, B. Sopori, K. VanSant and P. Basore, *Prog. Photovolt: Res. Appl.*, 2016, DOI: 10.1002/pip.2776.
23 A. K. A. Kelly, *et al.*, *Process for Transferring a Thin-Film Structure to a Temporary Carrier*, *US* 6143117, 2000.
24 G. J. Sullivan, M. K. Szwed and M. C. F. Chang, Method of Transferring a Thin Film to an Alternate Substrate, *US* 5391257, 1995.
25 S. G. Deutscher and E. Grunbaum, Method of Producing Monocrystalline Semiconductor Films Utilizing An Intermediate Water Dissolvable Salt Layer, *US* 4255208, 1981.
26 A. J. Shuskus and M. E. Cowher, Method for Removing Semiconductor Layers from Salt Substrates, *US* 4537651, 1985.
27 C. H. Lee, J. H. Kim, C. Zou, I. S. Cho, J. M. Weisse, W. Nemeth, Q. Wang, A. C. T. van Duin, T. S. Kim and X. Zheng, *Sci. Rep.*, 2013, **3**, 2917.
28 E. A. G. Hamers, M. N. van den Donker, B. Stannowski, R. Schlatmann and G. J. Jongerden, *Plasma Processes Polym.*, 2007, **4**, 275.
29 C. H. Lee, D. R. Kim, I. S. Cho, N. William, Q. Wang and X. Zheng, *Sci. Rep.*, 2012, **2**, 1000.
30 Y. Zhou, T. M. Khan, J. C. Liu, C. Fuentes-Hernandez, J. W. Shim, E. Najafabadi, J. P. Youngblood, R. J. Moon and B. Kippelen, *Org. Electron.*, 2014, **15**, 661.
31 I. G. Samatov, B. R. Jeppesen, A. N. Larsen and S. K. Ram, *Appl. Phys. A*, 2016, **122**, 458.
32 M. Vetter, J. Andreu, J. P. Borrajo, A. Martin, J. A. Rodriguez, O. Agustsson, J. Schotsaert, K. Bittkau, R. Carius, A. Gordijn, A. Hoffmann, I. M. Macedo, J. K. Rath, R. E. I. Schropp, A. Antony, J. Bertomeu and F. Kail, Proc. 26th Europ. Photovoltaic Solar Energy Conf. & Exh., Hamburg, Germany, 2011.
33 http://gwyddion.net/documentation/user-guide-en/statistical-analysis.html.
34 A. Shah, *Thin-film silicon solar cells*, EPFL Press, 2010, (p. 224, p. 324, p. 329).
35 Lumerical Solutions, Inc., http://www.lumerical.com/tcad-products/fdtd/.
36 V. E. Ferry, M. A. Verschuuren, M. Claire van Lare, R. E. I. Schropp, H. A. Atwater and A. Polman, *Nano Lett.*, 2011, **11**, 4239.
37 M. G. Deceglie, V. E. Ferry, A. P. Alivisatos and H. A. Atwater, *Nano Lett.*, 2012, **12**, 2894.

38 A. Tamang, A. Hongsingthong, P. Sichanugrist, V. Jovanov, M. Konagai and D. Knipp, *IEEE J. Photovoltaics*, 2014, **4**, 16.
39 D. C. Larson, in *Experimental methods in the preparation and measurement of thin films, Solid State Physics (Vol. 11, Methods of Experimental Physics)*, ed. R. V. Coleman, Academic Press, New York and London, 1974, ch. 12, p. 622.
40 M. J. Stowell, in *Defects in epitaxial deposits, Epitaxial Growth (Part B)*, ed. J. W. Matthews, Academic Press, New York and London, 1975, ch. 5, p. 437.
41 G. A. Salvatore, N. Münzenrieder, C. Barraud, L. Petti, C. Zysset, L. Büthe, K. Ensslin and G. Troester, *ACS Nano*, 2013, **7**, 8809.
42 B. Pantchev, P. Danesh, U. Kreissig and B. Schmidtz, *Opto-Electron. Rev.*, 2001, **9**, 43l.
43 M. Oliva-Ramirez, M. Macías-Montero, A. Borrasa and A. R. González-Elipe, *RSC Adv.*, 2016, **6**, 3778.
44 A. Tamang, A. Hongsingthong, V. Jovanov, P. Sichanugrist, B. A. Khan, R. Dewan, M. Konagai and D. Knipp, *Sci. Rep.*, 2016, **6**, 29639.
45 R. Dewan, S. Fischer, V. B. Meyer-Rochow, Y. Özdemir, S. Hamraz and D. Knipp, *Bioinspiration Biomimetics*, 2012, **7**, 016003.
46 S. Thiyagu, Z. Pei and M.-S. Jhong, *Nanoscale Res. Lett.*, 2012, **7**, 172.
47 C.-M. Hsu, C. Battaglia, C. Pahud, Z. Ruan, F.-J. Haug, S. Fan, C. Ballif and Y. Cui, *Adv. Energy Mater.*, 2012, **2**, 628.
48 D. Desta, S. K. Ram, R. Rizzoli, M. Bellettato, C. Summonte, B. R. Jeppesen, P. B. Jensen, Y.-C. Tsao, H. Wiggers, R. N. Pereira, P. Balling and A. N. Larsen, *Nanoscale*, 2016, **8**, 12035.
49 P. Kowalczewski, M. Liscidini and L. C. Andreani, *Opt. Express*, 2013, **21**, A808.
50 T. Matsui, H. Sai, T. Suezaki, M. Matsumoto, K. Saito, I. Yoshida and M. Kondo, Proc. 28th European Photovoltaic Solar Energy Conference, 2013, p. 2213.
51 M. A. Green, K. Emery, Y. Hishikawa, W. Warta and E. D. Dunlop, *Prog. Photovolt: Res. Appl.*, 2016, **24**, 3.
52 M. Stuckelberger, R. Biron, N. Wyrsch, F.-J. Haug and C. Ballif, *Renewable Sustainable Energy Rev.*, 2016, DOI: 10.1016/j.rser.2016.11.190.
53 S. K. Ram, S. Kumar and P. Roca i Cabarrocas, *Phys. Rev. B: Condens. Matter*, 2008, **77**, 045212.
54 A. Belfar, *Sol. Energy*, 2015, **114**, 408.
55 B. von Roedern, *Mater. Res. Soc. Symp. Proc.*, 2001, **668**, H6.9.1.
56 P. Chaudhuri, S. Ray, A. K. Batabyal and A. K. Barua, *Sol. Energy Mater. Sol. Cells*, 1994, **36**, 45.
57 *Handbook of optical constants of solids*, ed. E. D. Palik, Academic Press, 1998.

